frontiers | Frontiers in Built Environment

TYPE Original Research
PUBLISHED 08 December 2025
DOI 10.3389/fbuil.2025.1711028

OPEN ACCESS

EDITED BY
Arturo Tena-Colunga,
Autonomous Metropolitan University, Mexico

REVIEWED BY
Alonso Gomez Bernal,
Autonomous Metropolitan University, Mexico
Phu-Anh-Huy Pham,
Duy Tan University, Vietnam

*CORRESPONDENCE
Emilio J. Medrano-Sánchez,
emilio.medranos@epg.usil.pe

RECEIVED 23 September 2025
REVISED 04 November 2025
ACCEPTED 17 November 2025
PUBLISHED 08 December 2025

CITATION
Medrano-Sánchez EJ and Fabian MC (2025) Challenges and solutions in reinforcing self-built homes: experiences from Villa Maria del Triunfo, Lima, Peru.
Front. Built Environ. 11:1711028.
doi: 10.3389/fbuil.2025.1711028

Challenges and solutions in reinforcing self-built homes: experiences from Villa Maria del Triunfo, Lima, Peru

Emilio J. Medrano-Sánchez[1]* and Magaly C. Fabian[2]

[1]Universidad San Ignacio de Loyola, Lima, Peru, [2]Universidad César Vallejo, Lima, Peru

This study assesses H-shaped steel profiles (W8 × 31) as a retrofit solution for self-built dwellings in the Human Settlement (AA.HH). Ciudad de Gosen, Villa María del Triunfo (Lima, Peru). A four-part workflow was applied: i. field diagnosis with the Peruvian National Institute of Civil Defense (INDECI, by its Spanish acronym) checklist to classify seismic vulnerability and document construction pathologies; ii. numerical modeling in "Extended Three-Dimensional Analysis of Building Systems" (ETABS) v18 under Peruvian Standard E.030 to characterize story drift, torsion, and center of rigidity; iii. retrofit design that anchors and welds W8 × 31 profiles along critical load paths; and iv. experimental verification at National University of Engineering (UNI) Materials Testing Laboratory (LEM) following Peruvian Technical Standard (NTP) 350.405:2019 on representative columns and beams. Retrofitted specimens reached the testing machine's maximum axial load of 686 kN (70,000 kgf) with only minor cracking between 245 and 324 kN (25,000–33,000 kgf), confirming concrete-steel compatibility and increases in stiffness and axial capacity. Given the limited number of numerical models and laboratory specimens, the findings were integrated in a descriptive way to show the consistency between the ETABS simulations and the composite behavior observed in the tests. These results position W8 × 31 profiles as a feasible, constructible option for seismic risk reduction in self-built contexts and provide a technical bridge toward guidelines, on-site protocols, and community training aligned with the Sustainable Development Goal (SDG) for safe, resilient, and inclusive housing.

KEYWORDS

construction innovation, structural safety, sustainable urban development, seismic engineering, infrastructure vulnerability, structural reinforcement, self-built houses

1 Introduction

Earthquake events over the last decade showed that informal or self-built housing bore a disproportionate share of human and material impacts across countries (Woo et al., 2024). In Turkey, the 2023 Kahramanmaraş event recorded about 50,000 deaths, with building-code non-compliance in the informal stock identified as a key factor behind the fatal collapse patterns (Woo et al., 2024). In Nepal, the 2015 sequence left 625,000 houses fully destroyed and 180,000 partially damaged, revealing the weakness of non-seismic-resistant constructions (Khattri, 2021). Regionally, Ecuador (2000–2021) reported 719,501 victims and economic losses of $1,344.8 billion, while 70% of dwellings in

TABLE 1 Impact of major earthquakes (2015–2025) on informal or self-built housing.

Region	Event	Human losses	Economic/Housing impact
Turkey	2023 Kahramanmaraş	50,000 deaths	$8.8 billion GDP loss; significant damage to over one million residential and industrial structures (Woo et al., 2024; Demirdag and Nirwansyah, 2024; Kırtel et al., 2024)
Nepal	2015 Earthquakes	Numerous casualties	Severe economic damage; 625,000 houses fully destroyed; 180,000 partially damaged (Khattri, 2021)
Ecuador	2000–2021 (general)	719,501 victims	$1,344.8 billion economic losses; 70% informal housing in high-risk areas with structural deficiencies (Morante-Carballo et al., 2024)

high-seismic-risk zones were informal and exhibited structural deficiencies (Morante-Carballo et al., 2024). In Turkey, losses also included an estimated GDP reduction of $8.8 billion and damage to over one million residential and industrial structures (Demirdag and Nirwansyah, 2024; Kırtel et al., 2024). For a concise comparison of these cases, see Table 1.

Beyond totals, the literature described specific vulnerability mechanisms. In Turkey, non-compliance with codes in the informal stock was directly linked to the severity of collapse in 2023 (Woo et al., 2024). In Ecuador, the prevalence of informal housing in critical zones together with structural detailing shortcomings was noted as a determinant of observed risk between 2000 and 2021 (Morante-Carballo et al., 2024). Additionally, the use of non-seismic-resistant materials (e.g., adobe) and an uneven transition to modern techniques sustained high exposure levels in various contexts (Tello et al., 2022). Short-lived economic shocks in housing markets were also reported, such as temporary rent increases without long-term persistence in certain national settings (Brata and Patnasari, 2024). Finally, some government responses demonstrated an ability to cushion losses through subsidies and income-recovery programs, as documented for Wenchuan 2008 (Park and Wang, 2017).

The trends observed at the global scale were also evident in Latin America and the Caribbean, where self-built housing became a widespread practice marked by the absence of preliminary studies, formal permits, and professional supervision (Dedeoglu, 2025; Trujillo et al., 2019). This condition was further worsened by the use of low-quality materials and deficient construction techniques, which undermined structural resistance to seismic events (Dedeoglu, 2025; Trujillo et al., 2019). In addition, the location of many houses in unsuitable terrains significantly increased exposure to risk (Dedeoglu, 2025).

Across the region, several studies highlighted the need for structural reinforcement measures as a priority strategy to reduce collapse risk (Velasquez et al., 2025; Murray et al., 2023). Likewise, the importance of technical education and professional supervision in construction processes was underlined as a decisive factor in reducing vulnerability (Trujillo et al., 2019; Goldwyn et al., 2021). At the policy level, the urgency of implementing risk reduction programs, including insurance mechanisms accessible to vulnerable communities, was also emphasized as a means to strengthen resilience against future disasters (Sarmiento and Torres-Muñoz, 2020).

Table 2 summarizes key findings reported in the literature on the seismic vulnerability of self-built housing in Latin America and the Caribbean, focusing on structural deficiencies, the impact of natural events, safety perception, and collapse risk.

The recognition of the high vulnerability of self-built housing in Latin America and the Caribbean opened the discussion towards structural retrofitting alternatives that have been investigated internationally over the past decade. These solutions were mainly focused on low-rise dwellings, aiming to enhance their seismic resistance through accessible techniques and alternative materials.

Among the studied alternatives, fiber-reinforced concrete (FRC) walls showed lateral behavior comparable to that of conventional reinforced concrete walls, with similar failure modes and hysteresis curves (Correal et al., 2022). Fiber-reinforced elastomeric isolators (FREI) exhibited deviations lower than 10% in effective horizontal stiffness and damping ratios compared to experimental benchmarks, confirming their effectiveness (Rofiq and Tavio, 2022). Another important development was the use of cross-laminated timber (CLT), where improved connections increased compressive load capacity, making it applicable to medium-rise buildings (Alinoori et al., 2020).

In addition, low-cost base isolators made from recycled materials and fibers delivered outstanding performance in reducing seismic forces, consolidating their role as a feasible option for affordable housing in developing countries (Rivas-Ordonez et al., 2024). Finally, treated bamboo used as reinforcement in concrete beams achieved a 310% increase in load capacity, although with lower ductility compared to steel (Karakus-Zambak and Celik, 2025).

Table 3 summarizes these retrofitting solutions and their most relevant quantitative results, providing a comparative overview of international advances in the seismic protection of low-rise housing.

Despite the international advances in retrofitting solutions for low-rise dwellings, the literature still revealed critical gaps concerning the application of H-shaped profiles and other metallic techniques in self-built housing under seismic contexts. First, a significant lack of studies was identified regarding the seismic performance of metallic connections under real earthquake conditions, which is crucial since defective connections may compromise the global resistance of structures (Yancai et al., 2024). In addition, little attention was given to the role of floor systems in the seismic response of metallic housing, particularly in thin-walled cold-formed steel structures, where shear walls were analyzed but floor systems were almost completely omitted (Baldassino et al., 2021; Zhou et al., 2022).

Another recurrent gap was related to the constructive deficiencies inherent in self-built housing, where the introduction of contemporary materials was not always accompanied

TABLE 2 Seismic vulnerability of self-built housing in Latin America and the Caribbean (2010–2025).

Aspect	Description
Structural deficiencies	Over 65% of self-built dwellings presented construction pathologies such as unreinforced walls and misaligned brickwork (Velasquez et al., 2025)
Impact of natural events	Heavy rains and other natural phenomena caused significant damage to self-built dwellings in coastal Latin America (Dedeoglu, 2025)
Safety perception	In Puerto Rico, confidence in informal construction practices decreased after the 2019–2020 earthquakes (Goldwyn et al., 2021)
Collapse risk	Heavy construction and the presence of open ground floors significantly increased collapse risk (Murray et al., 2023)

TABLE 3 International retrofitting solutions for low-rise housing (2010–2025).

Solution	Evaluated parameter	Quantitative result
Fiber-reinforced concrete walls	Lateral performance	Similar to conventional reinforced concrete (Correal et al., 2022)
Fiber-reinforced elastomeric isolators	Horizontal stiffness deviation	Less than 10% (Rofiq and Tavio, 2022)
Cross-laminated timber reinforcement	Compressive load capacity	Improved; applicable to medium-rise buildings (Alinoori et al., 2020)
Low-cost base isolators	Reduction of seismic forces	Excellent performance; viable for low-cost housing (Rivas-Ordonez et al., 2024)
Bamboo reinforcement	Load capacity increase	310% increase in load capacity (Karakus-Zambak and Celik, 2025)

TABLE 4 Research gaps on metallic techniques in self-built housing (2010–2025).

Identified gap	Implication	Reference
Lack of studies on metallic connections under seismic conditions	Defective connections reduce global structural resistance	Yancai et al. (2024)
Neglect of floor systems in metallic housing	Limited understanding of global seismic response due to omission of floor systems	Baldassino et al. (2021), Zhou et al. (2022)
Constructive deficiencies in self-built housing	Use of contemporary materials without proper techniques increases vulnerability	Tello et al. (2022)
Limitations in displacement-based design methods (DDBD)	Insufficient knowledge of displacement responses across performance levels	Xie et al. (2024)
Limited research on alternative connection systems	Techniques such as clinching or ballistic nails not adapted to self-built housing	Fiorino et al. (2017)

by proper construction techniques, thus increasing seismic vulnerability (Tello et al., 2022). Likewise, the application of displacement-based design methods (DDBD) to self-built metallic systems remained limited, as there was insufficient research on displacement responses across different performance levels (Xie et al., 2024). Finally, the literature also showed limited exploration of alternative connection systems such as clinching or ballistic nails, which were mainly restricted to modular industrialized construction rather than applied to self-built housing (Fiorino et al., 2017).

Taken together, these gaps emphasized the need to expand research on the seismic behavior of metallic profiles in self-built housing, to develop normative frameworks and technical guidelines adapted to vulnerable contexts, and to promote training programs that strengthen structural safety in self-construction environments (Table 4).

Following the discussion on international research gaps in metallic retrofitting techniques, it is essential to examine the Peruvian context, particularly in Lima and other regional cities. In San Juan de Lurigancho, the evaluation of 30 self-built houses using the FEMA-P154 methodology indicated that 31% of the units had a collapse risk greater than 50%, leading to the proposal of welded mesh as a seismic reinforcement (Rojas et al., 2025). In Villa María del Triunfo, the assessment of 120 dwellings through the Benedetti-Petrini and FEMA P-154 methods reported improvements in shear strength ranging from 19% to 30% after the incorporation of welded wire mesh reinforcement (Tipacti and Rivas, 2025).

In the Cercado de Lima, the application of Rapid Visual Screening of Buildings (FEMA P-154) to public institutions showed that more than 60% were highly likely to experience significant structural damage during an earthquake (Calixto et al., 2023). In San Miguel, Puno, experimental tests demonstrated axial compression

TABLE 5 Seismic vulnerability and retrofitting proposals for self-built housing in Peru (2010–2025).

Location	Number of houses	Methodology	Key findings	Retrofitting proposals
San Juan de Lurigancho, Lima	30	FEMA-P154	31% with collapse risk > 50%	Welded mesh to improve seismic behavior
Villa María del Triunfo, Lima	120	Benedetti-Petrini, FEMA P-154	Shear strength improved by 19%–30%	Welded wire mesh reinforcement
Cercado de Lima, Lima	N/A	FEMA P-154	60% of public institutions with high probability of damage	N/A
San Miguel, Puno	N/A	Experimental tests	Axial compression and shear values below code minimums	N/A
Huancán, Mantaro Valley	30	INDECI	40% very high vulnerability, 50% high, 10% moderate	Structural reinforcements required
Lurigancho-Chosica, Lima	15	RNE, ETABS, STERA 3D	Good performance of confined masonry under severe earthquakes	Confined masonry housing design

and diagonal shear values below the minimum required by the Peruvian construction code, which substantially increased seismic vulnerability (Tarque and Pancca-Calsin, 2022).

In Huancán, Mantaro Valley, the evaluation of 30 houses carried out by INDECI revealed that 40% had very high vulnerability, 50% high, and 10% moderate, with irregularities in plan, height, and mass distribution being decisive factors (Trujillo et al., 2019). Finally, in Lurigancho-Chosica, the structural design of a three-story confined masonry house, modeled under Peruvian National Building Code (RNE), ETABS, and STructural Earthquake Response Analysis – 3D (STERA 3D) standards, demonstrated satisfactory seismic performance under severe earthquakes (Lenin et al., 2025). For a detailed summary of these findings and their reinforcement proposals, (see Table 5).

Building on international and regional evidence, the AA.HH. Ciudad de Gosen in Villa María del Triunfo offered a representative context to assess whether a purpose-designed steel retrofit reduced seismic vulnerability in self-built housing. The study addressed a recurrent condition: masonry with stiffness deficits and detailing shortcomings that increased interstory drift and torsional demand, particularly in buildings with plan irregularities and insufficient confinement. An applied approach was adopted that integrated field diagnosis, numerical modeling under the Seismic Design Standard E.030 (Peru), and experimental verification, aiming to appraise the suitability of H-shaped steel profiles (W8 × 31) anchored and welded along critical load paths. On this basis, the study sought to determine the extent to which the retrofit improved effective stiffness and axial capacity in representative elements and thereby reduced vulnerability. It was hypothesized that the intervention would significantly increase stiffness and strength, with specific expectations of mitigated stiffness asymmetries, increased stiffness under lateral demand, and higher compressive resistance without substantive ductility penalties within the evaluated range. The intended contribution was technical and constructability evidence to support guidelines and protocols for safe and progressive adoption in vulnerable settings in Lima and the wider region.

In parallel, recent scientific and practical contributions on the retrofitting of self-built housing have revealed significant progress. In Latin America, a housing model based on renewable timber has been developed, allowing for component disassembly and reuse, while promoting community participation and progressive housing adaptation to socio-economic conditions (Piantanida et al., 2022). In China, an indicator system integrating the Internet of Things and artificial intelligence was introduced to assess housing sustainability, enhance supervision, and improve early warning mechanisms, thereby strengthening safety and resilience (Sun and Zeng, 2025). In Colombia, various retrofitting strategies for adobe structures have demonstrated reductions in seismic damage, evaluated through sustainability indicators tailored to local conditions (Park and Wang, 2017).

These contributions are directly aligned with the Sustainable Development Goals (SDGs). The promotion of inclusive, safe, and resilient housing responds to SDG 11: Sustainable Cities and Communities (Essien, 2022). The use of sustainable materials and the reinforcement of resilience against natural disasters are linked to SDG 13: Climate Action (Ahmed, 2023). Finally, the development of affordable solutions for low-income communities connects with SDG 10: Reduced Inequalities, helping to improve quality of life and reduce social gaps (Ahmed, 2023). Within this framework, the present research aims to contribute empirical evidence on the application of metallic profiles in self-built housing, integrating these lessons into the local context.

This article documented i. numerical evaluations in ETABS of three representative self-built dwellings under Peruvian Standard E.030 seismic load combinations, and ii. a laboratory program of monotonic axial compression on concrete–steel composite specimens representative of the retrofitted joints. The retrofit considered H-shaped W8 × 31 steel profiles anchored with welded plates, epoxy and mechanical anchors at the critical locations identified in the vulnerability survey. Results were presented descriptively as interstory drifts and torsion from the models, and peak axial loads and observed cracking from the tests, and were compared qualitatively to show consistency of

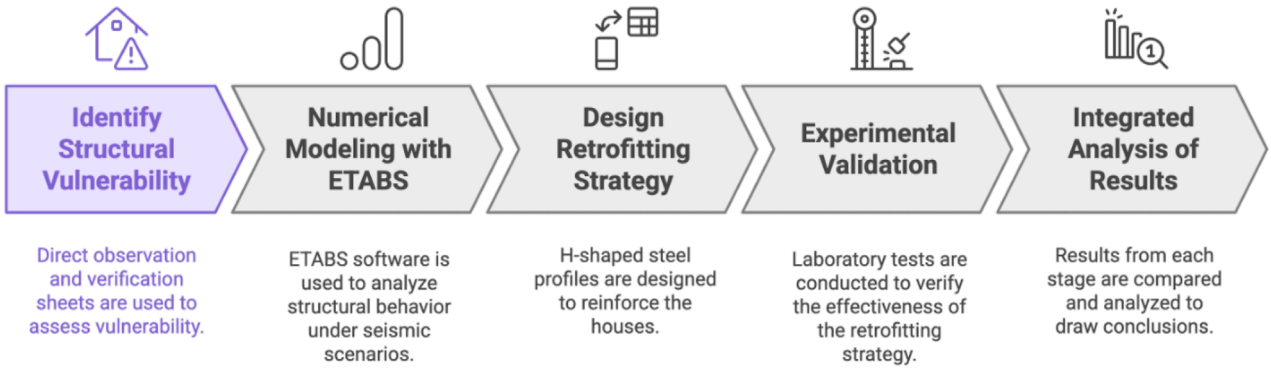

FIGURE 1
Flowchart of the research methodological design.

the retrofit mechanism. The scope did not include cyclic or dynamic testing, non-linear time-history analyses, cost or life-cycle assessments, or community acceptance studies; these aspects are outlined in Section 6.2 as directions for future work.

Within this scope, the contribution is to operationalize a low-cost W8 × 31 steel-profile retrofit for self-built dwellings, combining vulnerability-based targeting, code-aligned ETABS modeling of global interstory drifts, and laboratory verification of concrete–steel composite action and anchorage.

2 Methodology

2.1 Research approach and design

In line with the objectives, this study follows an applied, multi-method case-study design that integrates field diagnosis, numerical modeling, and element-level experimental verification. Rather than a controlled quasi-experiment, the design documents baseline conditions and, when available, contrasts pre- and post-retrofit numerical indicators (e.g., interstory drifts, torsion, eccentricities) derived from ETABS models. The workflow comprises: 1. classification of seismic vulnerability with the INDECI checklist; 2. 3-D modeling under the Peruvian Seismic Design Code E.030 (RNE) to characterize the structural configuration and derive inputs for the retrofit; 3. development of an H-shaped steel retrofit (W8 × 31) designed with American Institute of Steel Construction (AISC) criteria and adapted to the as-built architecture; and 4. laboratory verification of representative columns and beams at UNI–LEM according to NTP 350.405:2019. This integrated strategy provides an objective basis for consistent comparison across stages while deferring quantitative outcomes to the *Results* section (Figure 1).

2.2 Population and sample

The study area consisted of self-built houses located in the Ciudad de Gosen human settlement, situated in Villa María del Triunfo, Lima. The research population included all self-built dwellings in this area, which are characterized by precarious structural conditions and high seismic vulnerability. From this population, a sample of three representative houses was selected through non-probabilistic convenience sampling. The selection was based on accessibility and predefined criteria, including the identification of critical structural deficiencies and the need for retrofitting. These units were deemed suitable for detailed analysis and the subsequent implementation of structural reinforcement strategies, thereby ensuring the validity of the results obtained (Figure 2).

In addition, the dwellings were selected according to explicit inclusion criteria: they had to be self-built and occupied, exhibit critical structural deficiencies representative of the settlement, and allow safe access for inspection and retrofitting. Houses that had undergone prior formal retrofitting or that did not meet minimum safety conditions for fieldwork were excluded.

2.3 Variables and operationalization

The study considered two main variables: structural vulnerability and structural reinforcement. Structural vulnerability was defined as the susceptibility of self-built houses to experience severe damage or collapse under seismic loads. It was operationalized through three dimensions: slenderness, drift, and resistance. Structural reinforcement was defined as the application of intervention strategies aimed at improving the structural safety of the dwellings, specifically through the use of H-shaped steel profiles.

The dimensions of each variable were translated into measurable indicators, which guided the development of evaluation instruments, the numerical modeling process, and the experimental tests. In this way, the operationalization of the variables provided the technical framework required to connect the specific objectives with the testing of the central hypothesis (Table 6).

2.4 Techniques and instruments

To implement the operational definitions, the study combined field techniques, numerical modeling, and laboratory testing with standardized instruments. First, direct on-site observation was

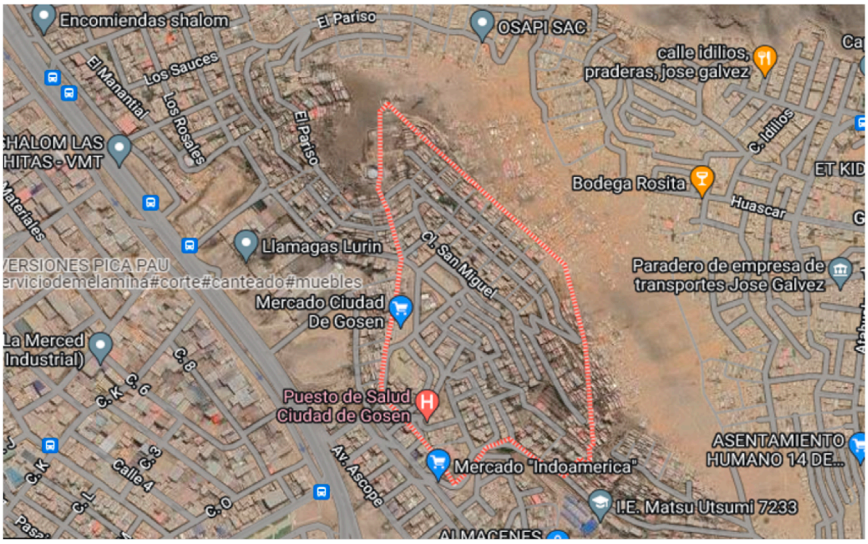

FIGURE 2
Geographical location of the Ciudad de Gosen human settlement, Villa Maria del Triunfo (VMT), Lima, Peru, selected as the study area.

TABLE 6 Operationalization of study variables.

Variable	Dimension	Indicator
Structural vulnerability	Slenderness	Ratio of wall height to thickness
	drift	Lateral displacement under seismic load
	Resistance	Compressive and shear strength of masonry
Structural reinforcement	Intervention design	Application of H-shaped steel profiles
	Performance	Improvement in structural safety after retrofitting

complemented with the INDECI verification sheet, an institutionally validated instrument that includes 12 critical items on seismic stability and safety in self-built housing; its application enabled the classification of seismic vulnerability and the systematic recording of construction quality, materials, foundations, and structural pathologies.

Second, three-dimensional structural models were developed in ETABS v18, reflecting the as-built configuration of the three dwellings. The models were subjected to seismic scenarios using parameters from the Peruvian Seismic Design Standard E.030, which permitted the estimation of center of rigidity, eccentricities, story drifts, and torsion for each floor. These outputs informed the H-profile retrofitting design, executed with AISC criteria and tailored to the existing architecture through calculations for member sizing and metal connections.

Third, an experimental program was conducted to verify the retrofitting effectiveness. Representative specimens were constructed to replicate real dimensions: three columns measuring $30 \times 30 \times 50$ cm with $f'_c = 20.6$ MPa (≈ 210 kg/cm^2) and two beams of 30×35 cm and 1 m in length. All specimens were retrofitted with W8 × 31 H-profiles, and the fabrication and finishing processes were documented, including welding and epoxy base coating. Finally, laboratory tests were performed at UNI's Materials Testing Laboratory (LEM) in strict accordance with NTP 350.405:2019, recording compressive strength, crack initiation, and failure to assess the retrofitting impact on stiffness and load capacity (Table 7).

2.5 Procedure

The methodological procedure was structured into four articulated phases that link field diagnosis, numerical modeling, retrofit design, and experimental verification. This section explains how each phase was executed and which inputs it produced for the next one, while avoiding any presentation of numerical outcomes, which are reported in the *Results* chapter.

2.5.1 Phase 1. field survey with the peruvian national institute of civil defense (INDECI, by its Spanish acronym) form and code check

Technical visits were carried out using the INDECI verification sheet together with the Peruvian building code criteria. Typical deficiencies were recorded, such as diagonal cracks, poorly resolved joints, absence of tying elements, and the use of hollow bricks

TABLE 7 Techniques and instruments applied in the study.

Technique/Instrument	Variable evaluated	Description	Standard/Source
INDECI verification sheet	Structural conditions	Official instrument including 12 critical items on seismic vulnerability, construction quality, materials, and pathologies	INDECI
Numerical modeling with ETABS v18	Seismic response	3D structural models simulating eccentricities, drifts, center of rigidity, and torsion of the dwellings	Peruvian Seismic Design Standard E.030
Experimental program (specimens with H-profiles)	Structural performance	Three columns (30 × 30 × 50 cm) and two beams (30 × 35 cm, 1 m) retrofitted with W8 × 31 H-profiles, welded and epoxy-coated	AISC criteria
Laboratory tests (UNI–LEM)	Strength and stiffness	Compressive strength tests monitoring crack initiation, failure, and stiffness under load	NTP 350.405:2019

TABLE 8 Summary of the INDECI verification sheet applied in field inspections.

Item evaluated	Description	Observed aspects during inspection
Structural system	Type and configuration of load-bearing walls, columns, and connections	Masonry units, presence of confined elements, quality of joints
Construction materials	Predominant materials used in walls, roofs, and reinforcements	Hollow bricks, concrete blocks, timber elements, or mixed systems
Pathologies	Visible deterioration or structural deficiencies	Cracks, separation between walls, irregular openings, moisture effects
Seismic provisions	Compliance with basic seismic-resistant criteria	Tie beams, vertical confinement, anchorage of roof structures
Non-structural elements	Condition of finishes and secondary components	Partition walls, ceilings, and façade elements susceptible to detachment

FIGURE 3
Most frequent nonconformities **(A)** Load-bearing walls with humidity; **(B)** Absence of structural elements; **(C)** Cracks in bearing wall.

as load-bearing walls. A concise overview of the instrument and its evaluated domains is provided in Table 8. Representative photographs of observed pathologies are shown in Figure 3, used solely as qualitative input for modeling.

2.5.2 Phase 2. ETABS modeling under code provisions

Based on plans and field findings, 3D structural models were built in ETABS v18. Seismic scenarios followed Standard E.030 and the applicable provisions for existing elements and masonry. The aim was to characterise the structural configuration and to produce input parameters for retrofit design, without reporting drifts, eccentricities, or torsion values. The code basis is summarised in Table 9, and representative ETABS models are depicted in Figure 4.

In addition to the as-built analytical models, a second set of ETABS models was developed in which the W8 × 31 steel profiles were explicitly incorporated at the joints selected in the vulnerability analysis. The layout adopted for Dwelling 1 (perimeter joints on grid lines A and C and the front joint on grid

TABLE 9 Code basis used for modeling, retrofitting design, and laboratory testing.

Standard/Guideline	Scope and application
Peruvian Seismic Design Standard E.030	Seismic parameters for ETABS scenarios; provisions for existing elements and masonry; global checks of drifts, torsion and eccentricities used in the numerical models
AISC (steel member and connection design)	Sizing and verification of H-shaped profiles (W8 × 31) and welded steel connections adapted to the existing architecture for the retrofitting scheme
Peruvian National Building Code (RNE)	General structural safety criteria applicable to self-built dwellings; complementary requirements referenced in the modeling and design stages
NTP 350.405:2019	Laboratory compressive testing procedure: specimen preparation, loading protocol, and registration of crack initiation, failure and stiffness under load

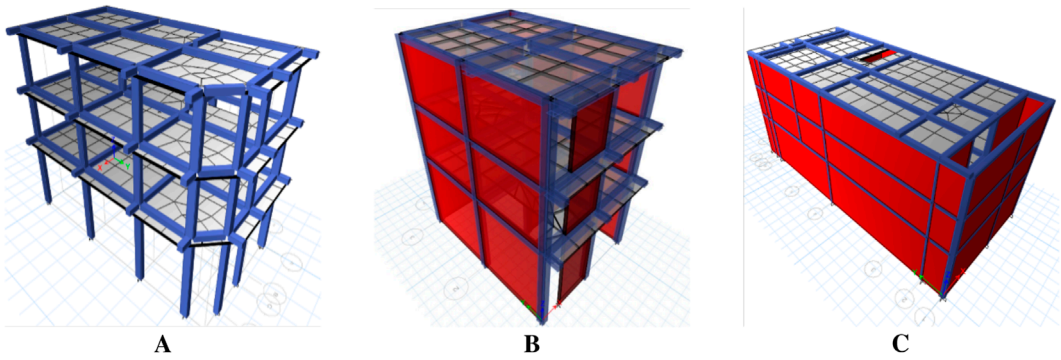

FIGURE 4
Representative ETABS models of the self-built dwellings used for numerical analysis: **(A)** 3D frame model showing beams–columns configuration; **(B)** 3D model 1 with masonry infills; **(C)** 3D model 2 with masonry infills.

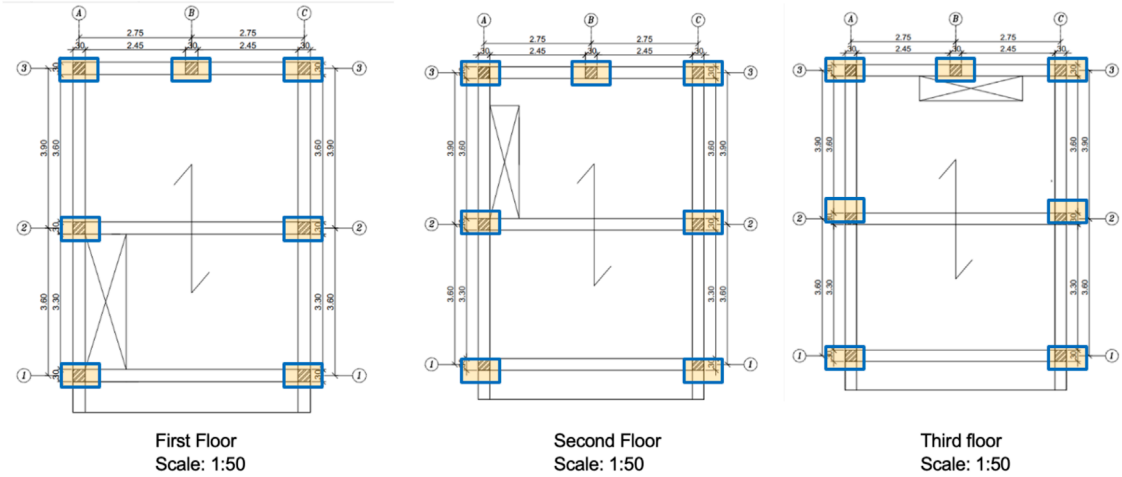

FIGURE 5
Plan view of Dwelling 1 showing the location of the W8 × 31 steel profiles at the perimeter joints on grid lines A and C, and at joint B–3, for the three storeys.

B–3), shown in (Figure 5), was used as the reference configuration and then adapted to Dwellings 2 and 3 according to their specific irregularities. These post-retrofit models were used to verify that the integration of the steel profiles increased the lateral stiffness and reduced both story drifts and torsional effects under the same E.030 seismic parameters.

TABLE 10 Modeling assumptions for Dwelling 1 (existing vs. retrofitted).

Parameter	Existing model	Retrofitted model
Support condition	Fixed base	Fixed base
Floor diaphragm	Rigid at each storey	Rigid at each storey
Concrete strength	f'_c = 20.6 MPa (210 kg/cm^2)	f'_c = 20.6 MPa (210 kg/cm^2)
Steel properties	–	A36 steel, f_y = 248 MPa (2,531 kg/cm^2), E_s = 200 GPa
Seismic combinations	E.030: $D + L + E_x$, $D + 0.25L + E_y$, 5% accidental torsion, P–Δ ON	Same E.030 combinations as existing model
Retrofit layout	–	W8 × 31 profiles at joints A, C, and B–3 for the three storeys (Figure 5)

To make the ETABS modeling assumptions explicit, the three dwellings were modeled in ETABS v18 with rigid floor diaphragms at each storey and fixed supports at the foundation level, according to the configuration documented during the field survey. Reinforced-concrete beams and columns were assigned a concrete compressive strength of f'_c = 20.6 MPa (equivalent to 210 kg/cm^2) and A36 steel reinforcement with a yield stress of f_y = 248 MPa (i.e., 2,531 kg/cm^2) and an elastic modulus of E_s = 200 GPa (i.e., 2.04×10^6 kg/cm^2). Masonry infill walls were represented as equivalent in–plane shell panels whose stiffness was derived from the INDECI vulnerability form. The seismic analysis followed the Peruvian Seismic Standard E.030, using the gravity–plus–earthquake load combinations,

$$D + L + E_x, \qquad D + 0.25L + E_y,$$

including 5% accidental torsion, and the geometric nonlinearity (P–Δ) was activated for the seismic load cases. This setting captures second-order geometric nonlinearity. In such conditions, P–Δ amplification is governed by the secant stiffness and is commonly summarized through a global stability index (θ), which clarifies how stiffness changes affect drift and stability (Hung et al., 2024; Anh et al., 2022).

For the retrofitted condition, a duplicate set of ETABS models was generated. In Dwelling 1 (the most critical case), W8 × 31 A36 steel profiles were introduced as steel frame elements at the perimeter joints on grid lines A and C and at the front joint B–3 on the three storeys, following the layout shown in (Figure 5); the same positioning rule was later adapted to Dwellings 2 and 3 according to their specific irregularities. Both the as–built and the retrofitted model sets were analysed under the same E.030 load combinations, which makes the before/after comparison of storey drifts and torsional ratios fully consistent (Table 10).

2.5.3 Phase 3: strengthening with H-profiles

In the third phase of the procedure, the structural strengthening proposal was developed using H-shaped steel profiles (W8X31). This method was designed as a technical solution applicable to the self-built houses of the sample, with the purpose of increasing their resistance to seismic demands.

The design consisted of placing H-profiles attached to the load-bearing masonry walls, fixed by epoxy bases and mechanical anchors. Subsequently, welding joints were carried out at critical intersections in order to ensure structural continuity. The arrangement of the profiles responded to reinforcement criteria in the most vulnerable zones identified during the initial inspection, such as corners and main load axes. The W8 × 31 profile was installed against the face of the load-bearing wall or the existing reinforced-concrete element. The joint was solved through vertically arranged mechanical anchors embedded in epoxy resin, ensuring force transfer to the resisting system.

In Dwelling 1, which was the most critical case, the strengthening layout was defined directly on the structural floor plans for the three storeys. H-shaped W8 × 31 profiles were placed at the perimeter joints on grid lines A and C on every storey, and an additional profile was installed at the front joint on grid B–3 to increase the lateral stiffness of the transverse frames and to mitigate the torsional effects detected in the seismic–static analysis. The same positioning criterion was later adapted to Dwellings 2 and 3 according to their specific vulnerability (Figure 5).

The construction process was complemented with protective surface finishes to prevent corrosion and ensure the durability of the system. The schematic representation of this procedure is shown in Figure 6.

2.5.4 Phase 4. specimen preparation and laboratory verification

In the fourth phase, retrofitted structural specimens were prepared for experimental laboratory verification. The specimens were fabricated according to the adopted design dimensions, which included representative columns and beams of the analyzed dwellings. For this phase, 30 × 30 × 50 cm and 30 × 30 × 100 cm reinforced-concrete elements were produced, with longitudinal reinforcement and stirrups, in order to reproduce the structural configuration observed in the self-built dwellings under study. The designed steel profile was attached to these elements using mechanical anchors and an epoxy base, thus forming the concrete–steel composite system to be verified in the laboratory (Figure 7). Throughout this process, fabrication details, connections, and surface finishes were documented to ensure fidelity with the proposed structural model.

The tests were conducted at UNI's Materials Testing Laboratory (LEM), following the protocol established by NTP 350.405:2019. These tests included compressive strength evaluation, observation of crack initiation, and registration of failure under controlled loading conditions. The methodological purpose of this stage was to assess the performance of retrofitted elements and validate the practical

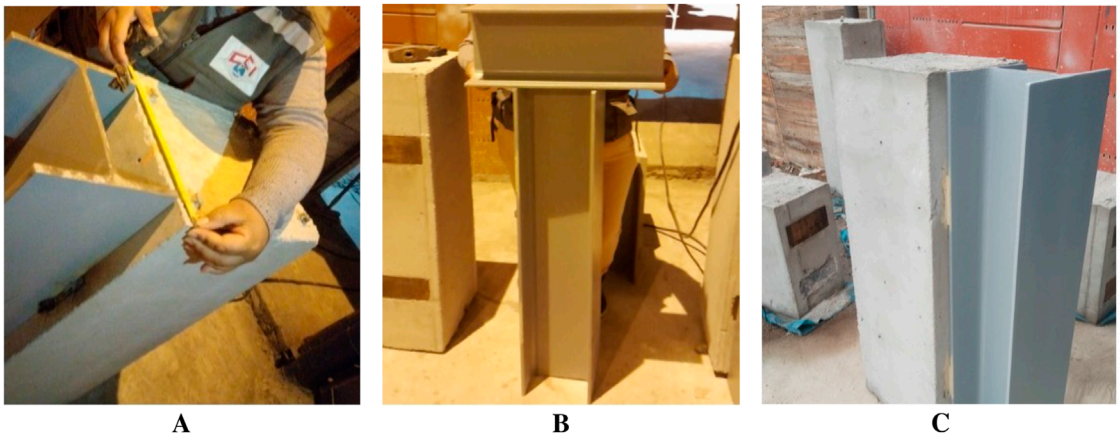

FIGURE 6
Phase 3 - retrofitting design with H-shaped profiles. **(A)** Measurement and dimensional verification of the H-profile for integration with the concrete element; **(B)** Assembly of the H-profile–column system, ensuring geometry and alignment; **(C)** Representative specimen with the installed H-profile and epoxy coating, prepared for constructability verification.

FIGURE 7
Manufacturing and assembly process for the concrete–steel composite system. **(A)** Type 1 column reinforcement (30 × 30 × 50 cm); **(B)** Type 2 column reinforcement (30 × 30 × 100 cm); **(C)** Type 1 and Type 2 reinforced-concrete columns.

applicability of the strengthening strategy under real construction scenarios (Figure 8).

During testing, the axial load was applied concentrically on the composite element, the reinforced-concrete specimen and the W8 × 31 steel profile acting together, using the upper and lower bearing plates of the UNI–LEM uniaxial testing machine (TOKYO KOKI SEIZOSHO; calibrated capacity 686 kN). In this set-up the steel profile was already fixed to the concrete face with mechanical anchors and epoxy, so the load path was common for both materials; therefore, all the strengths reported in Section 3.4 refer to the complete concrete–steel system and not to the concrete core alone.

These axial tests were conceived to validate the composite action assumed in the numerical models, not to measure the lateral stiffness directly. The ETABS simulations in Phase 2 had already shown that, once the W8 × 31 profiles are integrated at the critical joints (Figure 5), the global lateral stiffness of the dwellings increases and story drifts and torsional effects are reduced under the E.030 seismic parameters. By confirming in the laboratory that the reinforced-concrete element and the attached steel profile can transmit load together through the epoxy base and the mechanical anchors, the axial tests provide the physical support for using those lateral-stiffness improvements reported by the analytical models.

The tests were stopped when the machine reached its maximum available load (686 kN or 70,000 kgf), which means that the recorded peak value was governed by the equipment capacity and not by premature failure of the retrofitted specimen. Hairline cracking observed between 245 kN and 324 kN did not compromise the integrity of the column and confirmed adequate composite action. A copy of the original laboratory report is provided as Supplementary Material for traceability of the test protocol and measurements.

FIGURE 8
Representative samples adapted and prepared for laboratory testing, showing the integration of the H-profile with reinforced concrete elements.

TABLE 11 Interstory drifts of self-built dwelling No. 1 before and after retrofitting with H-shaped W8 × 31 profiles.

Story	Drift X (unretrofitted)	Drift Y (unretrofitted)	Drift X (retrofitted)	Drift Y (retrofitted)	E.030 limit
1	0.006898	0.017912	0.000463	0.000025	0.007
2	0.011782	0.026554	0.000499	0.000045	0.007
3	0.016853	0.027012	0.001971	0.000325	0.007

2.6 Descriptive results of seismic performance

The three-story self-built dwelling No. 1 showed, in its original (unretrofitted) condition, interstory drifts above the admissible limit of the Peruvian Seismic Design Standard E.030 ($\Delta_{max} = 0.007$). In the *Y* direction, drifts of 0.017912, 0.026554 and 0.027012 were obtained for the first, second and third story, respectively, which confirmed the torsional behavior and the lack of lateral stiffness in that direction. In the *X* direction, drifts also increased with height, reaching 0.006898, 0.011782 and 0.016853 for the first, second and third story, respectively. These values support the initial diagnosis of high seismic vulnerability.

After introducing the steel retrofitting system with H-shaped W8 × 31 profiles, and re-running the model in ETABS v18, interstory drifts decreased markedly in both directions. For the three stories, drifts in the *X* direction were reduced to 0.000463, 0.000499 and 0.001971, while in the *Y* direction they were reduced to 0.000025, 0.000045 and 0.000325, all of them well below the 0.007 limit established by E.030. This reduction shows that the retrofit increased the lateral stiffness of the system and controlled the torsion observed in the original model. The values are summarized in Table 11.

Besides complying with the code limit, the direct comparison between the "unretrofitted" and the "retrofitted" conditions shows that, in the most critical direction (*Y*), the third-story drift dropped from 0.027012 to 0.000325, which represents a reduction of more than one order of magnitude for this dwelling. Therefore, the descriptive results confirm that the adopted H-profile scheme is effective to reduce the seismic response of the analyzed dwelling.

These descriptive results were taken as the reference for the subsequent discussion on seismic performance and on the applicability of the H-profile system to self-built dwellings.

2.7 Ethical considerations and safety

All inspections were conducted with homeowners' authorization and with identity protection. Photographs were used solely for academic purposes, and location references were anonymized. No destructive tests were performed on occupied dwellings; representative specimens were fabricated specifically for the laboratory, following reference dimensions, and tested at the LEM under established safety protocols. Compliance with the applicable standards for design and testing (E.030, AISC, and NTP 350.405:2019) was ensured at all times, including proper handling of materials and waste according to laboratory procedures. No conflicts of interest were declared, and data integrity was guaranteed from field recording through laboratory processing.

3 Results

This chapter reports empirical findings in the same sequence as the methodological design. We present the field seismic-vulnerability diagnosis using the INDECI checklist (Phase 1), the

TABLE 12 Seismic vulnerability in self-built dwellings of AA.HH. Ciudad de Gosen (2023).

Item	Category	No. of dwellings	% of dwellings
01	Very high	0	0.00%
02	High	1	33.33%
03	Moderate	2	66.67%
04	Low	0	0.00%
Total	—	3	100.00%

numerical response of the dwellings modeled in ETABS under Code E.030 (Phase 2), the H-profile retrofit design (Phase 3), and the laboratory verification according to NTP 350.405:2019 (Phase 4). Finally, Section 3.5 reports the descriptive comparison between the numerical models and the laboratory verification.

3.1 Phase 1: field seismic-vulnerability diagnosis (INDECI)

Applying the INDECI verification sheet to three dwellings in AA.HH. Ciudad de Gosen yielded one "High" case (33.33%) and two "Moderate" cases (66.67%), with no "Very high" or "Low" records (Table 12). The most frequent deficiencies were diagonal cracks in load-bearing walls, deficient beam–column joints, absence of seismic joints, and use of hollow bricks as bearing walls (Figure 3). Based on this consolidated appraisal, Dwelling 01,showing the most severe findings, was prioritized for retrofit design and implementation.

3.2 Phase 2: ETABS structural modeling under code provisions

In the second phase, corresponding to the structural modeling in ETABS under the provisions of Standard E.030, differentiated results of drift and torsion were obtained for the three analyzed dwellings. *Dwelling 1* recorded a maximum drift of 0.016853 at the third floor in the X direction, together with a torsion value of 1.540 at the same level. For *Dwelling 2*, the highest demand was also observed at the third floor in the X direction, with a drift value of 0.038931, while torsion reached 1.154 at the second floor. Finally, *Dwelling 3* exhibited considerably lower drift values, with a maximum of 0.004593 at the third floor in the X direction; however, it showed the highest torsion among all dwellings, with a value of 1.639 recorded at the first floor. These findings identify Dwelling 2 as the building with the largest relative deformations, whereas Dwelling 3, although less demanding in terms of drift, revealed a more critical torsional behavior at the lower levels (Table 13).

3.3 Phase 3: structural retrofitting with H-profiles

In the third phase, representative elements were retrofitted with W8 × 31 H-profiles, following AISC criteria and using an epoxy coating to improve bond and provide corrosion protection. For experimental verification, three columns and two beams were fabricated to replicate the scaled dimensions of the intervened case: columns 50 × 30 × 30 cm and beams 100 × 35 × 30 cm. The consolidated dimensions are reported in Table 14, which supplies the quantitative basis for the subsequent laboratory testing. Figure 6 illustrates the measurement, mounting, and integration of the H-profile on the concrete members, confirming the constructability of the proposed system.

3.4 Phase 4: laboratory verification of compressive strength

In the fourth phase, axial compression strength tests were conducted at UNI's Materials Testing Laboratory (LEM), following the NTP 350.405:2019 standard. The tests were applied to reinforced-concrete elements that incorporated the W8 × 31 profile fixed according to the procedure described in the previous phase; therefore, the reported results correspond to the behavior of the concrete–steel composite system. Three cubic specimens of 30 × 30 × 50 cm reinforced with H-shaped profiles (W8 × 31) were tested, representing the columns of the surveyed dwellings.

The results showed good structural performance. Specimen M-1 exhibited the first minor crack at 245 kN (25,000 kgf) but maintained its integrity without collapse under the maximum load of 686 kN (70,000 kgf). Specimen M-2 did not show critical cracking or collapse at the maximum load, confirming the reinforcement's effectiveness. Finally, specimen M-3 exhibited a first minor crack at 324 kN (33,000 kgf, collapsing only at the maximum load, which suggests an adequate integration between the concrete and the H-profile.

These findings are summarized in Table 15, while Figure 9 illustrates the arrangement of the specimens and the behavior observed during the tests.

3.5 Phase 5: descriptive comparison of numerical and experimental results

Given the number of dwellings (three case studies) and laboratory specimens (five elements), the analysis of this stage was framed as descriptive. The objective was to show that i. the numerical retrofitting scheme with H-shaped W8 × 31 profiles effectively reduced interstory drifts and torsional effects in the most vulnerable dwelling, and ii. the laboratory tests confirmed that the concrete–steel composite element can safely transmit the axial loads assumed in the models.

3.5.1 Numerical response (Dwelling 1)

Table 16 already showed that, in the *unretrofitted* condition, Dwelling 1 exceeded the admissible interstory drift of the Peruvian Seismic Design Standard E.030 ($\Delta_{max} = 0.007$) in both directions. In the *Y* direction, the model obtained drifts of 0.017912 (1st story), 0.026554 (2nd story) and 0.027012 (3rd story), while in the *X* direction the values were 0.006898, 0.011782 and 0.016853 for the first, second and third story, respectively. These values confirmed

TABLE 13 Maximum drift and torsion values of the three dwellings modeled in ETABS.

Dwelling	Critical drift (direction, floor)	Value	Maximum torsion (floor)
Dwelling 1	X direction, 3rd floor	0.016853	1.540 (3rd floor)
Dwelling 2	X direction, 3rd floor	0.038931	1.154 (2nd floor)
Dwelling 3	X direction, 3rd floor	0.004593	1.639 (1st floor)

TABLE 14 Dimensions of retrofitted specimens used in laboratory testing.

Specimen	Height (cm)	Width (cm)	Thickness (cm)
Column 1	50	30	30
Column 2	50	30	30
Column 3	50	30	30
Beam 1	100	35	30
Beam 2	100	35	30

the lack of lateral stiffness and the torsional tendency previously identified in the vulnerability survey.

After introducing the steel retrofitting system with H-shaped W8 × 31 profiles and re-running the ETABS v18 model under the same E.030 load combinations, the interstory drifts decreased markedly in both directions. In the *X* direction the drifts were reduced to 0.000463 (1st story), 0.000499 (2nd story) and 0.001971 (3rd story); in the *Y* direction they were reduced to 0.000025, 0.000045 and 0.000325 for the three stories, all of them well below the 0.007 limit. This means that the retrofitted configuration not only met the code limit but also controlled the torsional effects of the original scheme.

To make this improvement explicit, the drift–reduction ratio R_Δ was computed as

$$R_\Delta = \frac{\Delta_{\text{unretrofitted}} - \Delta_{\text{retrofitted}}}{\Delta_{\text{unretrofitted}}} \times 100\ (\%).$$

For the most critical case (3rd story, *Y* direction) the ratio was

$$R_\Delta = \frac{0.027012 - 0.000325}{0.027012} \times 100 \approx 98.8\%.$$

Therefore, for the critical dwelling and the most unfavorable direction, the descriptive comparison shows a drift reduction close to 99%, which is consistent with the intended increase of lateral stiffness.

Because P–Δ was activated in the seismic cases, the post-retrofit stiffness increase implies a smaller P–Δ amplifier (lower θ) and therefore improved global stability, which is consistent with analytical interpretations of second-order effects reported in Hung et al. (2024) and Anh et al. (2022).

3.5.2 Experimental response (axial tests)

The axial compression tests carried out at UNI's Materials Testing Laboratory (LEM) on the retrofitted specimens (concrete element plus welded W8 × 31 profile, fixed with epoxy and mechanical anchors) reached peak loads between 245 kN and 324 kN, with minor cracking at the concrete cover. The test was stopped when the machine reached its maximum available load of 686 kN, which indicates that the ultimate value recorded in the manuscript was governed by the equipment capacity and not by premature failure of the composite column. This observation supports the assumption made in the numerical models that the concrete–steel system works integrally and can transfer axial forces through the epoxy base and the anchors. Table 15 reports, for specimens M-1, M-2 and M-3, the load at first visible cracking (245 kN for M-1, 324 kN for M-3, and none reported for M-2), the common maximum load of 686 kN, and the corresponding cracking pattern observed in each test.

However, this axial setup reproduced only a monotonic compressive demand. It did not simulate cyclic, reversed, or lateral seismic actions; therefore, the laboratory results must be read as a verification of concrete–steel composite action and load transfer capacity, rather than as a full validation of seismic performance. For this reason, Table 16 reports percentage drift reductions for the numerical models, while Table 15 presents absolute peak loads in the axial tests; no percentage 'capacity gain' is reported because unretrofitted twin specimens were not tested.

3.5.3 Consistency between models and tests

Taken together, the descriptive numerical results (Table 11) and the laboratory measurements confirm the same engineering message: once the W8 × 31 profiles are integrated at the critical joints identified in the vulnerability survey (Figure 5), the lateral stiffness of the dwelling increases and the torsional effects are reduced under the E.030 seismic parameters. The laboratory tests provide physical support for using these stiffness improvements reported by the analytical models.

4 Discussion

This discussion is based on descriptive evidence, because the research considered three representative self-built dwellings and five laboratory specimens. Within this scope, the findings indicate dimension-dependent effects of H-shaped steel profiles (W8 × 31) on seismic vulnerability. In Phase 2, ETABS modeling revealed critical interstory drifts and torsional effects that required intervention (Table 13); this is consistent with reports on informal

TABLE 15 Results of axial compression tests on cubic specimens reinforced with H-shaped profiles (W8 × 31).

Specimen	Description	First crack load (kN)	Max. load (kN)	Crack pattern/Observation
M-1	Cubic specimen 30 × 30 cm, H = 50 cm, reinforced with W8 × 31	245	686	First minor crack at 245 kN; no collapse under maximum load
M-2	Cubic specimen 30 × 30 cm, H = 50 cm, reinforced with W8 × 31	–	686	No critical cracking or collapse under maximum load
M-3	Cubic specimen 30 × 30 cm, H = 50 cm, reinforced with W8 × 31	324	686	First minor crack at 324 kN; no collapse under maximum load

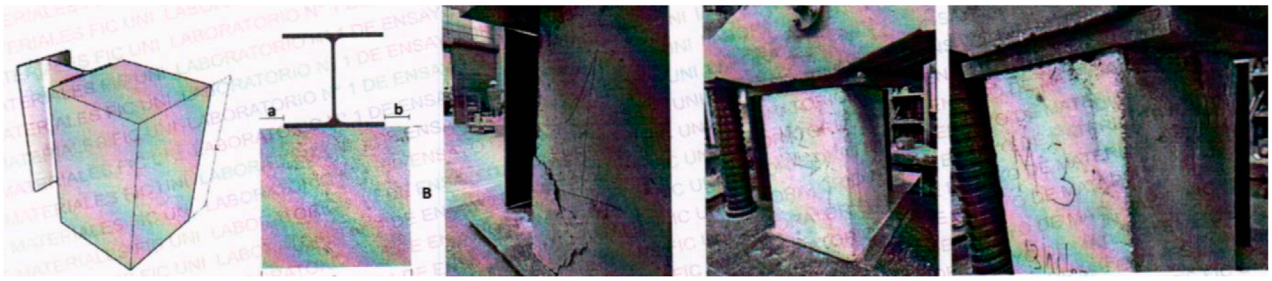

FIGURE 9
Representative photographs of the axial compression tests on cubic specimens reinforced with H-shaped profiles (W8 × 31): specimen configuration with the H-profile; specimen M-1 with initial crack; specimen M-2 under maximum load; specimen M-3 showing cracking pattern under load.

TABLE 16 Interstory drifts of Dwelling 1 before and after retrofitting with H-shaped W8 × 31 profiles, with percentage reduction.

Story	Drift *X* (unretrofitted)	Drift *Y* (unretrofitted)	Drift *X* (retrofitted)	Drift *Y* (retrofitted)	Reduction *X* (%)	Reduction *Y* (%)
1	0.006898	0.017912	0.000463	0.000025	93.2879	99.8604
2	0.011782	0.026554	0.000499	0.000045	95.7647	99.8305
3	0.016853	0.027012	0.001971	0.000325	88.3048	98.7968

housing affected by plan irregularities, lack of confinement and limited technical supervision (Woo et al., 2024; Morante-Carballo et al., 2024). In Phase 4, axial compression tests confirmed concrete–steel compatibility, achieving 686 kN (70,000 kg) with controlled initial cracking (Table 15), which provides experimental anchoring consistent with international interventions emphasising continuity and failure-mode control (Correal et al., 2022; Rofiq and Tavio, 2022).

The descriptive comparison of Phase 5 showed that varying the slenderness and the distribution of the W8 × 31 members did not change the qualitative trend of the response. In this manuscript, "slenderness" refers to the geometric proportion of the retrofitted element; its clear height relative to its effective thickness; within this descriptive comparison, greater slenderness coincided with the same qualitative response trend. The steel scheme contributed to homogenizing the stiffness of the retrofitted elements and to reducing the asymmetries that regional studies associate with plan irregularities and the absence of diaphragms in self-built housing (Trujillo et al., 2019; Murray et al., 2023). This observation is consistent with reports that highlight the role of welded joints and mechanical anchors in compensating local discontinuities and improving the global load path of mixed masonry–concrete systems (Yancai et al., 2024).

It must also be noted that the experimental evidence corresponded to static axial loading, while the numerical evidence corresponded to seismic-type load combinations under Peruvian Standard E.030. This means that the two fronts are complementary: the laboratory tests confirmed the integrity of the composite column and the effectiveness of welded/mechanical anchorage, and the ETABS models quantified the expected reduction of drifts and torsional effects once the W8 × 31 profiles are integrated.

Conversely, the observed relationship between slenderness and *stiffness* is coherent with solutions that restore effective confinement; for instance, FRC walls achieve lateral response

comparable to RC when reinforcement governs hysteresis and damage (Correal et al., 2022). Similarly, fibre-reinforced elastomeric isolators report < 10% deviations in effective horizontal stiffness (Rofiq and Tavio, 2022), and CLT with improved connections increases compressive capacity (Alinoori et al., 2020); all emphasise detail-level measures that modulate load transfer in low-rise dwellings. Quantitatively, in the most critical case (Dwelling 1, 3rd story, Y), the drift reduced from 0.027012 to 0.000325 (≈98.8%, Table 16), which is much larger than the < 10% effective-stiffness deviations typically targeted by fibre-reinforced elastomeric isolators (Rofiq and Tavio, 2022).

Regarding *strength*, the observed consistency with prior experiences on low-cost base isolation (demand reduction) (Rivas-Ordonez et al., 2024) and bamboo reinforcement (capacity gains up to 310% with ductility penalties) (Karakus-Zambak and Celik, 2025). Unlike the latter, the metallic scheme avoided severe ductility penalties via controlled welds and anchors, consistent with design recommendations for metallic connections in seismic contexts (Yancai et al., 2024; Fiorino et al., 2017).

At the regional scale, the drift and torsion patterns observed in the three analysed dwellings are consistent with diagnoses in Latin America and the Caribbean that attribute high vulnerability to heterogeneous materials, open ground floors, and lack of technical oversight (Dedeoglu, 2025; Trujillo et al., 2019; Morante-Carballo et al., 2024). This supports implementable, scalable steel-profile retrofits in self-built environments, aligned with policy measures for risk reduction/transfer and safe housing (SDGs 11 and 13) (Sarmiento and Torres-Muñoz, 2020; Essien, 2022; Ahmed, 2023). Complementarily, progressive housing with renewable materials and community participation provides routes for social and environmental sustainability (Piantanida et al., 2022; Sun and Zeng, 2025).

5 Conclusion

The study demonstrated that the incorporation of H-shaped steel profiles (W8 × 31) in self-built dwellings markedly increases structural stiffness and axial compressive strength. Both numerical modeling and laboratory testing confirmed the compatibility between steel and concrete, reducing structural vulnerability without compromising system ductility. Quantitatively, in the most critical case, the interstory drift decreased from 0.027012 to 0.000325 (≈ 98.8%, Table 16). These conclusions are preliminary within the scope of linear numerical modeling and monotonic axial tests.

It was observed that the H-shaped W8 × 31 retrofitting scheme reduced interstory drifts in the three analysed dwellings, according to the numerical results reported in Tables 11, 16. In these cases, greater slenderness of the reinforced members coincided descriptively with higher stiffness and with the axial capacity measured in the tests, consistent with the intended effect of the W8 × 31 scheme for self-built contexts.

The findings support the feasibility of implementing metallic profiles as a practical reinforcement alternative in vulnerable housing, while also highlighting the importance of complementing these measures with technical supervision and community training. Furthermore, the research opens opportunities to scale up this type of intervention towards broader housing programs, aligned with the Sustainable Development Goals on safety, resilience, and the reduction of urban inequalities.

6 Limitations and future work

This chapter integrates both the scope considerations of the study and the perspectives emerging from its results. The identified limitations should not be interpreted as shortcomings, but rather as methodological decisions that allowed the analysis to focus on critical variables of stiffness, strength, and structural distribution. From this focus, clear opportunities arise to extend the experimental and analytical framework, guiding future research toward a broader range of scenarios and evaluation variables.

6.1 Limitations

The study focused on a limited sample of three dwellings and on an experimental program based on static axial compression of representative specimens. This scope provided controlled and rigorous evidence on the behavior of W8 × 31 H-shaped profiles under specific conditions. In particular, the laboratory phase was restricted to monotonic axial compression; cyclic, hysteretic, or lateral testing was not included in this stage, so the seismic demand was represented through numerical modeling and not through experimental cycling. Consistently with this scope, the numerical and laboratory results were interpreted with descriptive statistics (ranges, direct comparisons) rather than with inferential tests. Without yet encompassing seismic response under cyclic loads or recorded ground motions. Similarly, structural modeling was carried out using linear assumptions, suitable for assessing initial improvements in stiffness and resistance, while future work could extend toward non-linear and inelastic analyses. Note that P–Δ was treated geometrically in ETABS, while material nonlinearity and cyclic degradation were not explicitly modeled; see Hung et al. (2024) and Anh et al. (2022) for broader nonlinear stability interpretations. High-fidelity finite-element simulations (ANSYS, ABAQUS) and cyclic or pseudo-dynamic tests were intentionally outside the scope, since the objective was to verify under controlled monotonic axial compression the concrete–steel composite action and the effectiveness of welded/mechanical anchorage, while linear ETABS models were used to estimate first-order changes in interstory drifts and torsion under Peruvian Standard E.030 seismic load combinations.

The INDECI checklist–based classification provided a standardized and institutionally validated framework, although it may be complemented in the future with alternative methodologies or higher-resolution instruments. Finally, the research did not fully address costs, life-cycle performance, or community acceptance, as the focus was placed on the technical validation of metallic reinforcement; these dimensions are best understood as opportunities for expansion rather than as strict limitations.

6.2 Future work

The findings of this research highlight the potential of H-shaped W8 × 31 steel profiles as an effective strategy to enhance the safety

of self-built dwellings. Building on this foundation, future studies may broaden the scope in several directions: assessing performance under dynamic seismic loads and cyclic tests; incorporating non-linear modeling to characterize secant stiffness, energy dissipation, and hysteretic degradation; and exploring design variations such as anchors, weld beads, or corrosion protection. Additionally, integrating cost–effectiveness assessments, life-cycle performance, and community perception will link the technical validation with the social and economic feasibility of implementation. These complementary lines of work strengthen the path toward developing technical guidelines and construction protocols applicable to similar contexts.

Finally, future studies should benchmark the ETABS results with high fidelity finite element analyses (ANSYS or ABAQUS) that capture geometric and material nonlinearity, connection detailing, and local buckling, and should complement them with larger scale cyclic or pseudo-dynamic tests. This combined numerical and experimental evidence would quantify ductility and energy dissipation, constrain failure modes, and strengthen the basis for design guidance in similar contexts.

Data availability statement

The raw data supporting the conclusions of this article will be made available by the authors, without undue reservation.

Ethics statement

Written informed consent was obtained from the individual(s) for the publication of any potentially identifiable images or data included in this article.

Author contributions

EM-S: Conceptualization, Data curation, Formal Analysis, Investigation, Methodology, Supervision, Validation, Visualization, Writing – review and editing. MF: Data curation, Formal Analysis, Investigation, Project administration, Resources, Software, Writing – original draft.

Funding

The authors declare that no financial support was received for the research and/or publication of this article.

Conflict of interest

The authors declare that the research was conducted in the absence of any commercial or financial relationships that could be construed as a potential conflict of interest.

Generative AI statement

The authors declare that no Generative AI was used in the creation of this manuscript.

Any alternative text (alt text) provided alongside figures in this article has been generated by Frontiers with the support of artificial intelligence and reasonable efforts have been made to ensure accuracy, including review by the authors wherever possible. If you identify any issues, please contact us.

Publisher's note

All claims expressed in this article are solely those of the authors and do not necessarily represent those of their affiliated organizations, or those of the publisher, the editors and the reviewers. Any product that may be evaluated in this article, or claim that may be made by its manufacturer, is not guaranteed or endorsed by the publisher.

Supplementary material

The Supplementary Material for this article can be found online at: https://www.frontiersin.org/articles/10.3389/fbuil.2025.1711028/full#supplementary-material

References

Ahmed, I. (2023). Addressing the impacts of inland floods on informal housing in honiara, solomon islands. *Adv. 21st Century Hum. Settlements* F631, 61–81. doi:10.1007/978-981-99-2248-2_4

Alinoori, F., Sharafi, P., Moshiri, F., and Samali, B. (2020). Experimental investigation on load bearing capacity of full scaled light timber framed wall for mid-rise buildings. *Constr. Build. Mater.* 231, 117069. doi:10.1016/j.conbuildmat.2019.117069

Anh, H. P. P., Yuen, T. Y., Hung, C. C., and Mosalam, K. M. (2022). Seismic behaviour of full-scale lightly reinforced concrete columns under high axial loads. *J. Build. Eng.* 56, 104817. doi:10.1016/j.jobe.2022.104817

Baldassino, N., Zordan, M., and Zandonini, R. (2021). Experimental study of the shear behaviour of floor diaphragms in light steel residential buildings. *Thin-Walled Struct.* 167, 108099. doi:10.1016/j.tws.2021.108099

Brata, A. G., and Patnasari, Y. (2024). Earthquakes and housing rental prices in urban indonesia: a hedonic price analysis. *Buletin Ekonomi Moneter Dan Perbankan/Monetary Banking Economics Bulletin* 27, 229–240. doi:10.59091/2460-9196.1746

Calixto, V., Cruz, C., and Huaco, G. (2023). "Seismic vulnerability of state educational infrastructures in cercado de lima, using the fema 154 methodology," in *9th international conference on innovation and trends in engineering, CONIITI 2023* (Bogotá, Colombia: 2023 Congreso Internacional de Innovación y Tendencias en Ingeniería (CONIITI)). doi:10.1109/CONIITI61170.2023.10324141

Correal, J. F., Carrillo, J., Reyes, J. C., Renjifo, A. E., and Herrán, C. A. (2022). Cyclic tests of full-scale fiber-reinforced concrete (frc) walls with steel and hybrid fibers for low-rise buildings. *Eng. Struct.* 256, 113952. doi:10.1016/j.engstruct.2022.113952

Dedeoglu, I. O. (2025). Evaluating earthquake-induced damage in hatay following the 2023 kahramanmaraş earthquake sequence: tectonic, geotechnical, and structural engineering insights. *Appl. Sci. Switz.* 15, 9704. doi:10.3390/app15179704

Demirdag, I., and Nirwansyah, A. W. (2024). Unravelling the economic impacts: forecasting the effects of the february earthquakes on türkiye's economy. *J. Regional City Plan.* 35, 21–43. doi:10.5614/jpwk.2024.35.1.2

Essien, E. (2022). Impacts of governance toward sustainable urbanization in a midsized city: a case study of uyo, nigeria. *Land* 11, 37. doi:10.3390/land11010037

Fiorino, L., Macillo, V., and Landolfo, R. (2017). Experimental characterization of quick mechanical connecting systems for cold-formed steel structures. *Adv. Struct. Eng.* 20, 1098–1110. doi:10.1177/1369433216671318

Goldwyn, B., Javernick-Will, A., and Liel, A. (2021). Dilemma of the tropics: changes to housing safety perceptions, preferences, and priorities in multihazard environments. *Nat. Hazards Rev.* 22, 04021012. doi:10.1061/(ASCE)NH.1527-6996.0000457

Hung, C. C., Pham, P. A. H., Yuen, T. Y., and Mosalam, K. M. (2024). Full-scale cyclic testing of slender rc columns bent in double curvature under high axial load. *J. Build. Eng.* 82, 108186. doi:10.1016/j.jobe.2023.108186

Karakus-Zambak, O., and Celik, O. C. (2025). Behavior of bamboo reinforced concrete (brc) beams under monotonic and dynamic loads. *Constr. Build. Mater.* 458, 139683. doi:10.1016/j.conbuildmat.2024.139683

Khattri, M. B. (2021). Differential vulnerability and resilience of earthquake: a case of displaced tamangs of tiru and gogane villages of central nepal. *Prog. Disaster Sci.* 12, 100205. doi:10.1016/j.pdisas.2021.100205

Kırtel, O., Aydın, F., Boru, E., Toplu, E., Aydın, E., Sarıbıyık, A., et al. (2024). Seismic damage assessment of under-construction industrial buildings: insights from the february 2023 Türkiye-Syria earthquakes. *Case Stud. Constr. Mater.* 21, e03507. doi:10.1016/j.cscm.2024.e03507

Lenin, B. R., Piero, G. R., Jerico, Y. P., and Malena, S. L. (2025). "Damage states and seismic performance levels of a three-story confined masonry structure, lima, peru (avestia publishing)," in *10th international conference on civil, structural and transportation engineering, ICCSTE 2025*. doi:10.11159/iccste25.351

Morante-Carballo, F., Santos-Baquerizo, E., Pinto-Ponce, B., Chacón-Montero, E., Briones-Bitar, J., and Carrión-Mero, P. (2024). Proposal for the rehabilitation of householsd in seismic vulnerability zones. *Int. J. Saf. Secur. Eng.* 14, 701–716. doi:10.18280/ijsse.140304

Murray, P. B., Feliciano, D., Goldwyn, B. H., Liel, A. B., Arroyo, O., and Javernick-Will, A. (2023). Seismic safety of informally constructed reinforced concrete houses in puerto rico. *Earthq. Spectra* 39, 5–33. doi:10.1177/87552930221123085

Park, A., and Wang, S. (2017). Benefiting from disaster? public and private responses to the wenchuan earthquake. *World Dev.* 94, 38–50. doi:10.1016/j.worlddev.2016.12.038

Piantanida, P., Villa, V., Vottari, A., Pilar, C., and Lando, A. (2022). Low-cost sustainable timber framed dismountable modular houses: concept and design guidelines (ISEC press). *6th Australasia South-East Asia Struct. Eng. Constr. Conf. ASEA-SEC-06 2022* 9. doi:10.14455/ISEC.2022.9(2).HOS-01

Rivas-Ordonez, F. S., Meza-Munoz, A. O., Madera-Sierra, I. E., Rojas-Manzano, M. A., Patino, E. D., Salmerón-Becerra, M. I., et al. (2024). Alternatives for enhancing mechanical properties of recycled rubber seismic isolators. *Polymers* 16, 2258. doi:10.3390/polym16162258

Rofiq, H., and Tavio, I. D. (2022). Model validation of carbon-fiber and glass-fiber reinforced elastomeric isolators using finite element method. *IOP Conf. Ser. Earth Environ. Sci.* 1116, 012001. doi:10.1088/1755-1315/1116/1/012001

Rojas, A. W. C., Villa, D. M. D., and Sánchez, G. Y. R. (2025). "Seismic vulnerability assessment using fema p-154 and welded mesh reinforcement in informal settlements in peru (avestia publishing)," in *10th international conference on civil, structural and transportation engineering, ICCSTE 2025*. doi:10.11159/iccste25.258

Sarmiento, J. P., and Torres-Muñoz, A. M. (2020). Risk transfer for populations in precarious urban environments. *Int. J. Disaster Risk Sci.* 11, 74–86. doi:10.1007/s13753-020-00252-3

Sun, G., and Zeng, H. (2025). Assessing critical risk factors to sustainable housing in urban areas: based on the nk-sna model. *Sustain. Switz.* 17, 6918. doi:10.3390/su17156918

Tarque, N., and Pancca-Calsin, E. (2022). Building constructions characteristics and mechanical properties of confined masonry walls in San miguel (Puno-peru). *J. Build. Eng.* 45, 103540. doi:10.1016/j.jobe.2021.103540

Tello, J., Cabrera, M., Rodríguez, J., and Eyzaguirre, C. (2022). Compressed earth blocks for rural housing in seismic zones using bagasse fibers from sugarcane. *Key Eng. Mater.* 922, 177–182. doi:10.4028/p-tsg594

Tipacti, D., and Rivas, G. Y. (2025). "Seismic vulnerability analysis using qualitative and quantitative methods and structural strengthening proposal for self-built dwellings in latin american informal settlements (avestia publishing)," in *10th international conference on civil, structural and transportation engineering, ICCSTE 2025*. doi:10.11159/iccste25.324

Trujillo, V. M. S., Herrera, R. G., Nolasco, G. C., Lara, C. M. G., and Carboney, J. A. A. (2019). Characterization of pathologies in housing structures. a case study in the city of tuxtla gutierrez, chiapas, mexico. *J. Build. Eng.* 22, 539–548. doi:10.1016/j.jobe.2019.01.014

Velasquez, H. A., Hurtado, S. D., and Angel, C. (2025). Impact of structural degradation on the seismic resilience of self-built housing: an approach based on intelligent circular resilience. *J. Build. Pathology Rehabilitation* 10, 123. doi:10.1007/s41024-025-00633-5

Woo, G., Gargiulo, M., Napolitano, F., Amoroso, O., Russo, R., and Capuano, P. (2024). Turkish earthquake death tolls: lessons from downward counterfactual analysis and informal construction. *Front. Earth Sci.* 12, 1376924. doi:10.3389/feart.2024.1376924

Xie, C., Wang, X., Vasdravellis, G., and Liang, W. (2024). Displacement profile for direct-displacement based seismic design of dual frame-wall resilient system. *J. Constr. Steel Res.* 214, 108495. doi:10.1016/j.jcsr.2024.108495

Yancai, H., Kusbiantoro, A., Ismail, A. H., and Lin, L. (2024). Structural damage model of steel structure connections with initial defects: a review. *J. Adv. Res. Appl. Mech.* 121, 163–186. doi:10.37934/aram.121.1.163186

Zhou, X., Yao, X., Xu, L., Shi, Y., Ke, K., and Liu, L. (2022). Shake table tests on a full-scale six-storey cold-formed thin-walled steel-steel plate shear wall structure. *Thin-Walled Struct.* 181, 110009. doi:10.1016/j.tws.2022.110009